J. Fluid Mech. (1997), *vol.* 332, *pp.* 247–262

Convection and flow in porous media. Part 2. Visualization by shadowgraph

By L. E. HOWLE[1] R. P. BEHRINGER[2] AND J. G. GEORGIADIS[3]

[1]Department of Mechanical Engineering and Materials Science, Duke University, Durham, NC 27708, USA,

[2]Physics Department, Duke University, Durham, NC 27708, USA

[3]Department of Mechanical and Industrial Engineering, University of Illinois at Urbana-Champaign, Urbana, IL 61801, USA

(Received 21 March 1996 and in revised form 9 July 1996)

We present results for pattern formation at the onset of convection in fluid-saturated porous media obtained by a novel variation on the shadowgraphic technique (modified shadowgraphic technique). Both ordered and disordered media are used, each exhibiting distinct behaviour. Ordered porous media are constructed from grids of overlapping bars. Convective onset in this type of medium is characterized by a sharp, well-defined bifurcation to straight parallel rolls. The orientation of the convection rolls is determined by the number of bar layers, N_b; odd N_b leads to rolls with axes perpendicular to the direction of the top and bottom bars, and even N_b to rolls at 45° to the bars. Disordered porous layers are produced by stacking randomly drilled disks separated by spacers. In this system, we observe a rounded bifurcation to convection with localized convection near convective onset. More specifically, the flow patterns take on one of several different three-dimensional cellular structures after each cycling through convective onset. These observations may be described by two different mechanisms: random spatial fluctuations in the Rayleigh number (Zimmermann *et al.* 1993), and/or spatial variation in the thermal conductivity on the length scale of the convection wavelength (Braester & Vadasz 1993).

1. Introduction

The present experiments are a continuation of the preceding study, Part 1, (Shattuck *et al.* 1997) to probe pattern formation and the accompanying heat flow for convection in a fluid-filled layer of porous medium. In the previous paper, we present experiments which utilize magnetic resonance imaging (MRI), a powerful tool which allows non-invasive determinations of the local density, velocity, and temperature of the fluid within a porous medium. This work also contains a survey of important issues regarding convective pattern formation in general and porous media convection in particular, and we refer the reader to it for definitions or parameters. Here, we show that simple porous media can be constructed which allow easy visualization of the patterns by shadowgraph. We refer to the use of a shadowgraph with these special media as a modified shadowgraph technique (MST) (Howle 1993; Howle, Behringer & Georgiadis 1993*a*,*b*). We present an exploration of several different kinds of media which exploit the MST. In the introduction of this work, we

consider two issues which pertain in particular to the present experiments: the effects of anisotropy and of horizontal variations in spatial properties.

From both sets of experiments emerge two related points: first, for dense fluids such as water, the ratio of pore size to layer height cannot be made effectively infinitesimal; and second, as a consequence, the structure of the medium leaves its imprint on the pattern selection process, and therefore on many details of the convective flow. The limits on the ratio of pore scale to layer height occur because of conflicting constraints: the fluid should obey the Boussinesq approximation, yet relaxation times must be small enough to carry out experiments over acceptible time scales. This situation is not a result of the way in which the media are constructed, but is linked intrinsically to the transport and thermodynamic properties of typical fluids, such as water. Consequently, the usual assumption of spatial uniformity may not be justified.

The rest of this work is structured as follows. In the following section, we discuss the experimental techniques used for this work, in particular the modified shadowgraphic method for pattern visualization in fluid-saturated porous media. We also discuss the inherent limitations on the Darcy number in convection experiments. We present experimental results for four different media in §3. These results indicate that the structure of the solid matrix plays a key role in the pattern formation and heat transport. Section 4 contains concluding remarks.

Before proceding to the discussion of the shadowgraph experiments, we briefly review recent work concerning the effects of anisotropy and of spatial parameter variation. In general, porous media need not be isotropic. The criterion for the onset of convection was extended to anisotropic media by Castinel & Combarnous (1975), Epherre (1975), and Kvernvold & Tyvand (1979). Kvernvold & Tyvand (1979) show, citing Epherre (1975), that onset to convection in anisotropic media occurs at the critical Rayleigh number

$$Ra_c = \pi^2 \left[\left(\frac{\eta}{\xi} \right)^{1/2} + 1 \right]^2 \tag{1.1}$$

with a corresponding wavenumber

$$q = \pi(\xi\eta)^{-1/4} . \tag{1.2}$$

Here, η is the ratio of the horizontal to the vertical permeability and ξ is the ratio of the horizontal to the vertical conductivity.

A related issue is the effect of spatial variations in such parameters as γ or κ_m on the convective flows. The most frequently studied non-uniformity is porosity variation near a boundary as in the work by Vafai (1984), and Amiri & Vafai (1994). However, we find that spatial variations throughout the medium may be important. Some information on this issue is available (Vincourt 1989; Néel 1990; Gounot & Caltagirone 1989; Zimmermann, Sesselberg & Petruccione 1993; Braester & Vadasz 1993).

Regarding spatial variations of γ and κ_m we contrast the recent work of Zimmermann *et al.* (1993) and of Braester & Vadasz (1993). Zimmermann *et al.* have shown in the context of the Swift–Hohenberg model (Swift & Hohenberg 1974) that random spatial fluctuations in the Raleigh number lead to localized modes and a rounded heat transport curve. Although the modes are localized and rounding appears in $Nu(Ra)$, the bifurcation is still sharp. Braester & Vadasz consider continuous spatial variations of γ and the thermal conductivity in the context of bifurcation theory.

The key point here is the existence of steady solutions, other than the conduction solution, for $Ra < Ra_c$ when γ and k_m, the thermal conductivity, vary spatially. If no-flow solutions do not exist below Ra_c, then the resulting weak flow will couple resonantly near Ra_c. The result will be an imperfect bifurcation, as seen for instance in experiments by rounding in the Nusselt curve. The existence of non-zero flow below onset depends only on the spatial form of k_m. Specifically, given the Darcy equation for steady flow

$$-\nabla P - (\mu/\gamma)\boldsymbol{v} + \rho \boldsymbol{g} = 0, \tag{1.3}$$

a necessary condition for a $\boldsymbol{v} = 0$ solution is that

$$\nabla \rho \times \boldsymbol{g} = 0. \tag{1.4}$$

Here, ρ depends only on the temperature profile $T(\boldsymbol{r})$, and the temperature profile is determined, through the heat equation, by k_m. The key point of their analysis is that horizontal spatial variations in k_m can be inconsistent with a no-flow solution at any Ra. The result is an imperfect bifurcation. Specifically, the normal form for the critical mode amplitude, A, has the form

$$\dot{A} = \epsilon A - A^3 + \beta, \tag{1.5}$$

where

$$\epsilon = (Ra - Ra_c)/Ra_c, \tag{1.6}$$

and β is a measure of the spatial projection of $k_m(\boldsymbol{r})$ on the critical mode. Since the convective contribution to the heat transport varies as A^2, the effect of β will be apparent in the dimensionless heat transport Nu.

There are important conceptual differences in the scenarios offered by Zimmerman *et al.* and by Braester & Vadasz. Specifically, the former indicate a sharp bifurcation to convection even though Nu should show rounding; the patterns are expected to be cellular rather than roll-like. The latter consider only roll-like solutions in the case in which a no-flow state is specifically excluded. Key to the differing models is an assumption about whether there is – or is not – a no-flow state for positive ΔT.

It seems likely that in the disordered media used in the present experiments both effects are present. Specifically, the disordered patterns observed here for our disordered media are consistent with the predictions of Zimmermann *et al.* (Indeed, their predictions provide an alternative explanation in general for the polygonal patterns reported in previous experiments.) However, there may be small horizontal temperature gradients in our experiments because of the differing conductivities of the fluid and solid. Hence, the rounding in the heat transport which we observe for disordered media may have its source in both effects.

2. Experimental method

The aim of the present experiments is to provide non-perturbative images of the convective planform in conjunction with high-resolution heat transport measurements. These data provide a test of both older theories, as well as a test of recent models which probe the effect of local parameter variation on pattern selection.

The primary difficulty in obtaining images of the convective pattern for porous media convection (PMC) is that the fluid and solid matrix generally do not share the same index of refraction, even if the latter is transparent. Consequently, in a typical porous medium constructed from spherical particles, light which enters the medium is rapidly diffused, thus making visualization by optical techniques ineffective. However,

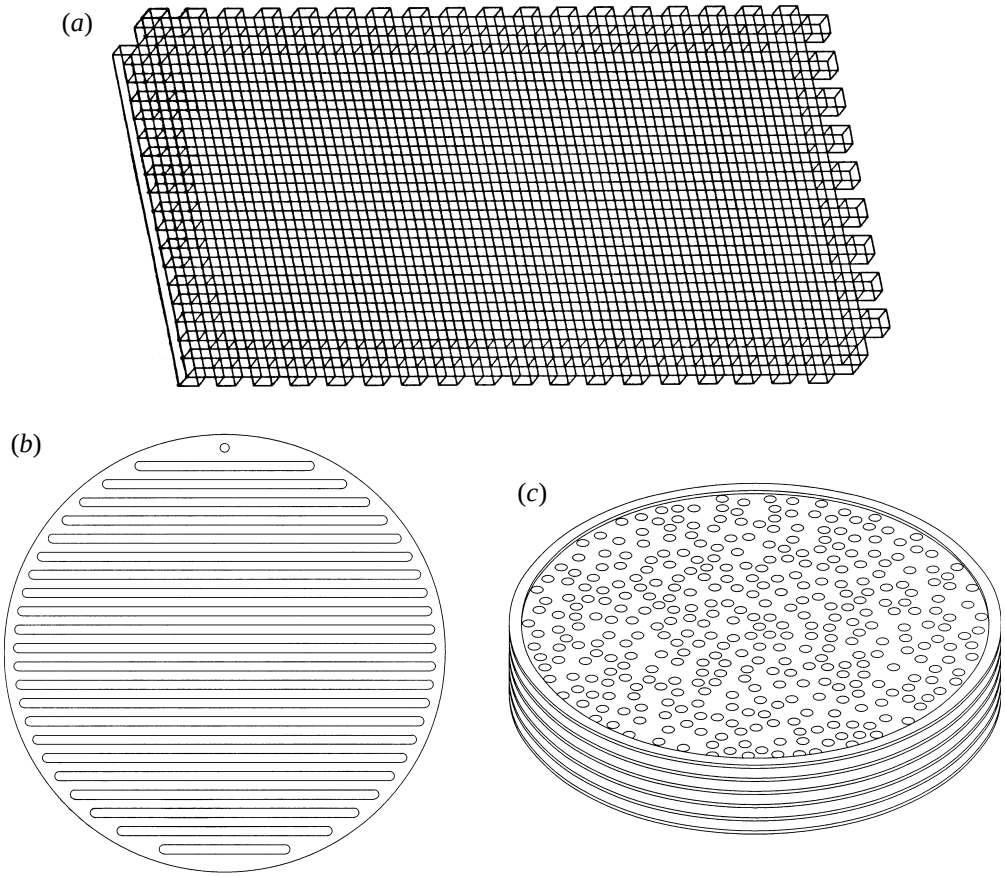

FIGURE 1. (*a*) Cell A: Scale drawing of the regular porous layer with rectangular sidewalls. (*b*) Cells B and C: Geometry of the bar medium with a cylindrical planform including the sidewalls. Each successive layer is rotated by $\pi/2$. (*c*) Cell D: Disordered porous medium consisting of five pseudo-randomly perforated discs separated by annular spacers.

it is possible to construct media with fluid–solid interfaces which are perpendicular or parallel to some direction of light travel. In this case, imaging with a shadowgraph is possible, even without any index matching. We refer to this construction as a modified shadowgraphic technique (MST) (Howle *et al.* 1993*a*, *b* and Howle 1993).

We have used two qualitatively different types of structures for the MST and many others are possible. Here, we present detailed results for four structures which represent two of these possible media. We will refer to these as cells A, B, C, and D; their properties are summarized in table 1.

The first general matrix for the MST, which we refer to as 'regular', consists of a periodic stacking of bars, as exemplified by figure 1(*a*) for cell A, which contains six layers. We have carried out additional experiments with five and seven (cell C) layers of bars. In experiments using regular media, the lateral boundaries have either rectangular cross-sections, like cell A, or circular cross-sections, like cells B and C. We describe in detail the structure of cell A. Other regular media differ only in the number of layers or in the shape or size of the lateral boundaries.

For cell A, each of six layers was constructed from 0.159 cm thick polycarbonate sheets. Slots, of 0.159 cm width were machined along the length of the sheet. The slots

were spaced two slot widths apart (centre to centre) so that the porosity of these media was $\phi = 0.5$. Alternate layers were rotated by 90° about the vertical axis relative to the immediate neighbouring layers. The third layer had the same orientation as the first but was offset by one half of the grid period. Similarly, the fifth layer was offset from the third, the second from the fourth, etc. This was repeated until the desired number of layers was reached. The offset of every other layer prevented the fluid from having an unimpeded path when traversing the layer vertically. The lateral dimensions of the layer were $L_x = 5.56$ cm and $L_y = 2.70$ cm. The medium height was $L = 0.902$ cm; hence the aspect ratios were $\Gamma_x = L_x/H = 6.16$ and $\Gamma_y = L_y/H = 2.99$ respectively.

We determined the medium permeability by measuring the flow rate through the medium of a viscous fluid, typically glycerin, versus pressure provided by a column of the fluid. We also determined the temperature of the fluid, since the viscosity of glycerin is strongly temperature dependent. We obtained data for fifteen column heights, and fitted these data to a line to obtain the permeability and to verify that the overall flow was Darcian.

We also determined the thermal conductivity of the water-saturated medium, except for cell A, by placing the saturated medium in a stabilizing thermal gradient and measuring the temperature difference across the layer versus the power input from a resistive heater. Measurements of both conductivity and permeability in the two characteristic directions of these media as shown in table 1. The tables show that the media are only slightly anisotropic in the sense of Kvernvold & Tyvand (1979) (i.e. vertical versus horizontal anisotropy). To obtain the conductivity of cell A we used a weighted average of the conductivities of the fluid and solid materials. We did this rather than measure the conductivity in a stabilizing thermal gradient because the containing walls (not shown in figure 1) transport a non-negligible fraction of the heat which was difficult to determine precisely.

Table 1 also contains information on the Darcy number, Da, and the Prandtl number, Pr. The latter is the porous-medium Prandtl number based on the vertical thermal diffusivity:

$$Pr_m = \frac{\nu}{\kappa_m}. \tag{2.1}$$

The porous thermal diffusivity is

$$\kappa_m = \frac{k_m}{(\rho c_p)_f} \tag{2.2}$$

where ρ and c_p are the density and specific heat at constant pressure of the fluid respectively and the subscripts m and f refer to medium and fluid respectively. We use specific heat data for water from Lide *et al.* (1993). The Darcy number is defined by

$$Da = \frac{\gamma_v}{H^2} \tag{2.3}$$

where γ_v is the vertical permeability.

We next turn to the construction of cells B and C. These media are identical in internal structure to the rectangular grid medium but the horizontal planform, as shown in figure 1(*b*), is cylindrical rather than rectangular. Cells B and C consist of six and seven bar layers respectively. The radius of each grid disk is 3.02 cm. The aspect ratios ($\Gamma \equiv radius/H$) are 3.35 for the six-layer medium, cell B, and 2.87 for the seven-layer medium, cell C.

	Cell A		Cell B		Cell C		Cell D	
Property	Horizontal	Vertical	Horizontal	Vertical	Horizontal	Vertical	Horizontal	Vertical
Permeability, γ (cm^2)	3.9×10^{-4}	2.6×10^{-4}	3.9×10^{-4}	2.6×10^{-4}	3.9×10^{-4}	2.6×10^{-4}	2.3×10^{-4}	1.8×10^{-4}
Conductivity, k_m (W cm^{-1} K^{-1})	not measured	$3.6 \times 10^{-3*}$	not measured	$3.6 \times 10^{-3*}$	not measured	$3.6 \times 10^{-3*}$	0.010	0.008
Size (cm)	5.56, 2.70	0.902	3.02 (radius)	0.902	3.02 (radius)	1.052	3.016 (radius)	1.056
Prandtl number, Pr_m	3.35		3.35		3.35		4.19	
Darcy number, Da	3.2×10^{-4}		3.2×10^{-4}		2.6×10^{-4}		1.6×10^{-4}	
Porosity, ϕ	0.5		0.5		0.5		0.314	

TABLE 1. Thermo-physical properties cells A, B, C and D.* estimated.

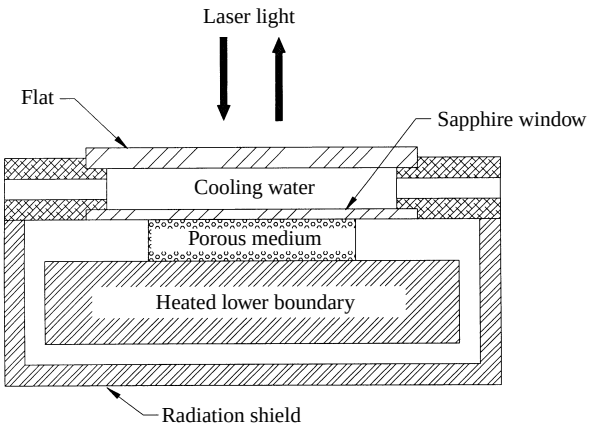

FIGURE 2. Experimental apparatus showing porous medium location and cooling water flow.

The final medium, cell D, has a disordered structure, as sketched in figure 1(*c*). This medium consists of disks with the same 0.159 cm thickness as the three other media. However, in this case, each disk has 362 non-overlapping 0.159 cm diameter holes (with some additional space around each hole) which are random-densely placed. We stacked all the disks together and drilled them simultaneously with the same set of holes. We then stacked a number of these disks together to form the medium. During assembly, we rotated each disk in the stack approximately 60° relative to its predecessor in the stack. Annular spacers 0.051 cm thick separate each of the five disks in this medium. Spacers also separate the disks from the upper and lower bounding surfaces. The porosity of each disk is 0.251. Including the void space created by the spacers, the net porosity of the disordered medium is 0.314. We list parameters of the disordered medium in table 1. Because we know the hole coordinates of each disk, we also know the spatial details of the medium. It is possible, in principle, to tune the gap between disks in order to eliminate the horizontal/vertical anisotropy in the permeability and/or conductivity. However, we have not attempted to do so in the media used here, because these anisotropies are relatively small.

The working fluid used for all experiments was distilled and deionized water. The water was degased before we filled the medium. Even with degased fluid, an experimental run had a limited lifespan, usually about one month, before small bubbles appeared. We stopped a run when bubbles first occurred.

We show a schematic of the experimental apparatus used for simultaneous thermal measurement and pattern visualization in figure 2. Thermal control of the upper boundary and the radiation shield is maintained by a recirculating bath which flows constant-temperature controlled water between the upper boundary of the porous medium (sapphire window in figure 2) and a crown glass optical flat. The advantage of sapphire over other transparent materials for use as a boundary is that the high thermal conductivity (0.40 W cm^{-1} K^{-1}) reduces horizontal thermal gradients at the boundary. A regulated thermal controller maintains the temperature at the upper boundary constant at 25.000°C $\pm$ 0.002°C.

We measure temperature with precision thermistors, eight of which are in thermal contact with the upper sapphire boundary and two of which are in thermal contact with the lower boundary. A scanning digital multimeter reads the resistance of the thermistors at specified time intervals and stores the data in a computer. The

resolution of the temperature measurements is ± 0.0003 K. In addition, we use a high-precision AC differential bridge circuit to monitor the temperature difference across the porous layer.

The lower boundary consists of an oxygen-free, high-conductivity copper block. A regulated voltage supply provides current to a heater which is glued to the lower boundary. Due to the very high conductivity of the copper block, we expect that the appropriate thermal boundary condition is one of constant temperature (Metcalf & Behringer 1991) rather than of constant heat flux. Specifically, horizontal thermal gradients are minimized at the boundary. The upper surface of the copper block (which contacts the medium) is flat to one half-wavelength of the laser light used for visualization, per inch. This surface is gold-plated in order to provide a highly reflective surface (99%) for visualization.

A 20 mW 632.8 nm He-Ne laser provides light for shadowgraphic visualization. The columated light passes through the optical flat, cooling water and sapphire before entering the saturated porous medium. Light then travels through the medium and reflects off the lower boundary before traversing the medium a second time. A computer-driven frame grabber acquires the image. By appropriately choosing the distance between the image plane and the medium we maximize the contrast in the image.

The porous medium is small enough that the vertical thermal diffusion time is only about 6 min. This means that the time required for the relaxation of fluid transients, once a change has been made in the power input, is less than an hour, except near a bifurcation point, where critical slowing down effects may occur.

3. Experimental results

We consider first experimental results obtained with the regular media, cells A–C, followed by those for the disordered medium, cell D. These results consist of data near onset of convection, including the critical Rayleigh number, the Nusselt number, the pattern at onset and the associated wavenumber. We also present results for secondary instabilities which occur well above the onset of convection. It is convenient in presenting these results to use the reduced Rayleigh number

$$R = Ra/Ra_c = 1 + \epsilon. \tag{3.1}$$

3.1. *Results for cell A*

The onset of convection in cell A, which has a rectangular horizontal planform and a regular bar structure, is characterized by a sharp change in the slope of the data for $Nu(Ra)$ and well-defined straight parallel convection rolls. To our knowledge, these data and those of Shattuck *et al.* (1994, 1995, 1997) are the first clear observations of a parallel roll convection pattern for PMC. Nusselt data for cell A are shown in figure 3(*a*). Within our resolution of about 0.1%, there is no rounding at the onset of convection, as emphasized by the expanded plot in figure 3(*b*).

The convection patterns for this cell, consisting of straight parallel rolls, are typified by figure 4, which pertains to $R = 1.93$. Similar patterns are observed from the smallest R, $R \simeq 1.05$, for which the pattern is discernable to $R \simeq 3.0$ at which point a secondary instability occurs. These patterns are notable for two reasons. First, although theoretically predicted near convective onset, parallel rolls are rarely observed. Most often patterns are polygonal (Lister 1990). Second, the rolls intersect the sidewalls at an angle of 45°, rather than 90° which is typical for Rayleigh–Bénard

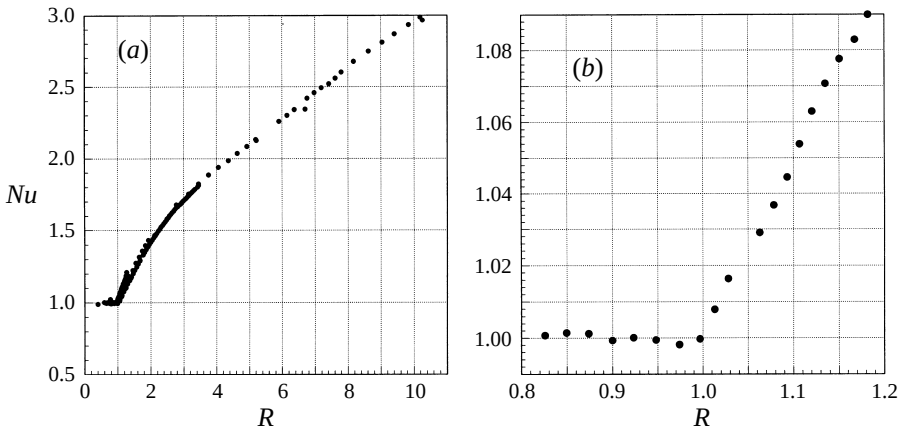

FIGURE 3. (*a*) Heat transfer data for five experimental runs with the rectangular planform grid medium (cell A). Onset of convection is observed at $Ra = 50 \pm 6$. The critical wavenumber in four of the runs is $q = 3.6 \pm 0.3$. (*b*) High resolution heat transfer data for cell A near the bifurcation to convection.

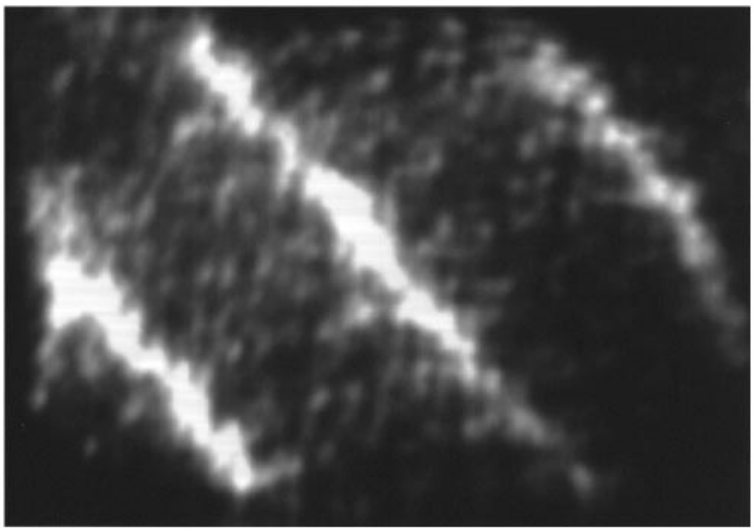

FIGURE 4. Typical steady wave pattern near the onset of convection in the rectangular grid porous medium, cell A. Here, $R = 1.93$ with $q = 3.6$.

convection (Cross 1982). We have observed both possible orientations of the rolls, i.e. slanting right to left or vice versa. An important issue is whether this intersection angle is caused by the boundaries or by the structure of the medium. The results for cells B and C, discussed below, indicate clearly that it is the structure of the medium which leads to the pattern orientations.

The critical ΔT for cell A is very well defined by the Nusselt curve. Using the value of ΔT at onset, the measured value of the permeability and the known properties of water and the polycarbonate, we obtain $Ra_c = 50 \pm 6$. The relatively large uncertainty in Ra_c is due primarily to the uncertainty in the thermal properties of the polycarbonate solid phase. This critical Rayleigh number disagrees somewhat with

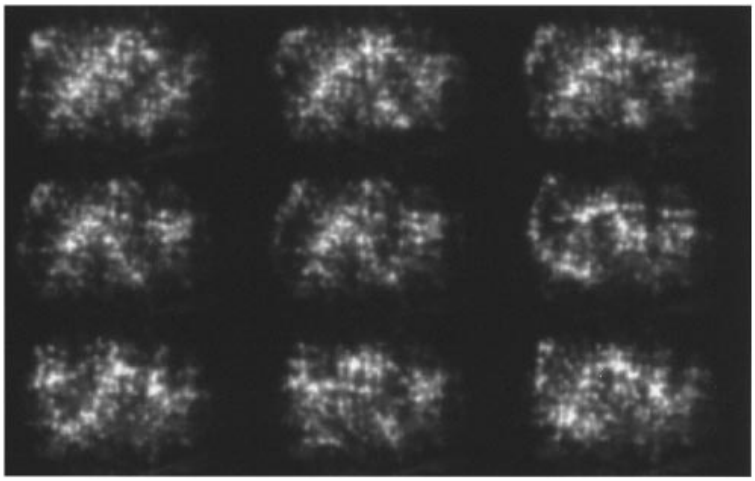

FIGURE 5. Example of temporally evolving patterns above $R = 3.5$, for cell A.

the predicted value of $Ra_c = 4\pi^2$ for a horizontally infinite homogeneous isotropic medium. A modest part of the difference between experiment and theory may be explained by the fact that cell A has a relatively small aspect ratio which would tend to elevate Ra_c (Beck 1972). We expect that the remainer of the difference is explained by the effects of the pore structure on the pattern selection process.

The wavenumber for the pattern in figure 4 is $q = 3.6 \pm 0.3$, which is the wavenumber which occurs most frequently in this medium. The relative difference, $\delta q/q$, between the measured and predicted q and the relative difference $\delta Ra_c/Ra_c$ between the measured and predicted Ra_c are comparable. An elevation of q could also account for the elevation of Ra_c. However, in one of five experimental runs with this system, we observed $q = 4.0 \pm 0.3$, with the rolls still oriented at 45° with respect to the sidewalls. (Each run corresponds to a complete replacement of the water and starts from $\Delta T = 0$.)

The stability of the steady pattern with increasing Ra was strongly wavenumber dependent. Patterns with $q = 3.6$ were generally stable to three-dimensional disturbances from onset to approximately $R = 3$. Above $R = 3.5$ the patterns were time dependent with complicated time series. For instance, figure 5 shows a typical patterns in the time-dependent regime which evolved from a steady pattern with $q = 3.6$. By contrast, the $q = 4.0$ pattern was stable to three-dimensional disturbances up to at least $R = 8$. This agrees, semi-quantitatively, with the wavenumber stability calculations by Straus (1974).

The slope of the Nusselt curve, $Nu(R)$ for R just larger than unity provides a simple measure of the strength of the convective flow just above onset. Referring to figures 3, we obtain a slope at onset

$$S \equiv \mathrm{d}Nu/\mathrm{d}R \tag{3.2}$$

of $S = 0.53 \pm 0.17$ in the convective region near onset. This should be contrasted to the prediction (Joseph 1976) of $S = 2.0$. The explanation for the difference between theory and experiments may lie with either the effects of finite H/d (including possible forcing from the periodic structure of the medium) or finite aspect ratio. In this regard,

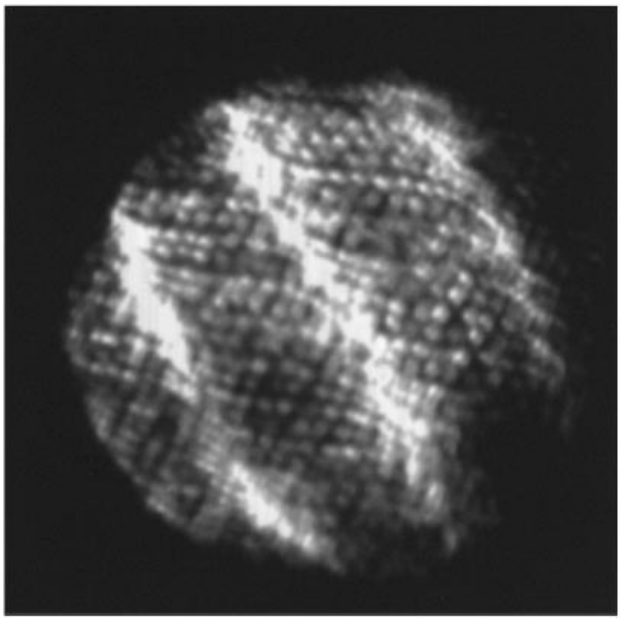

FIGURE 6. Slightly supercritical ($R = 1.29$) convection pattern for cell B (six layers). The roll orientation for this case is 45° relative to the grid directions.

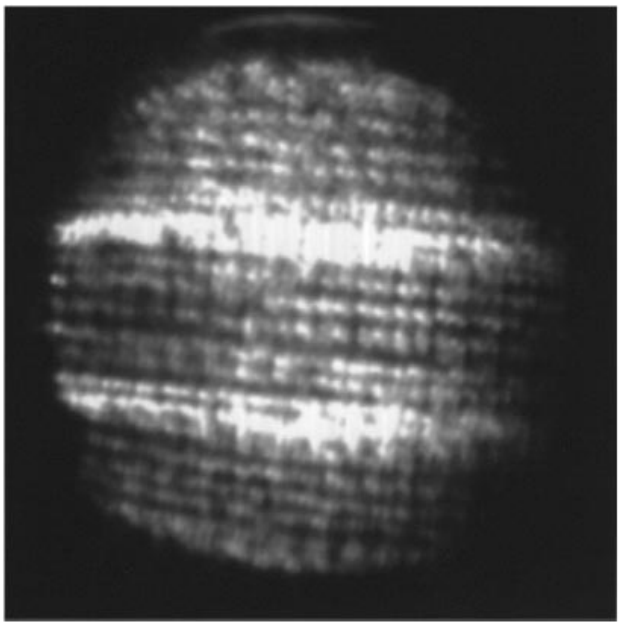

FIGURE 7. Convection pattern in Cell C (seven layers). An odd number of layers produces patterns which align with the grid.

we note that several other experiments have yielded slopes which are low compared to this prediction. These include Elder (1967) who found $S \simeq 1.0$, Shattuck *et al.* (1994, 1995) who found $S = 0.78$, and Close, Symons & White (1985) who found that S decreased with H/d.

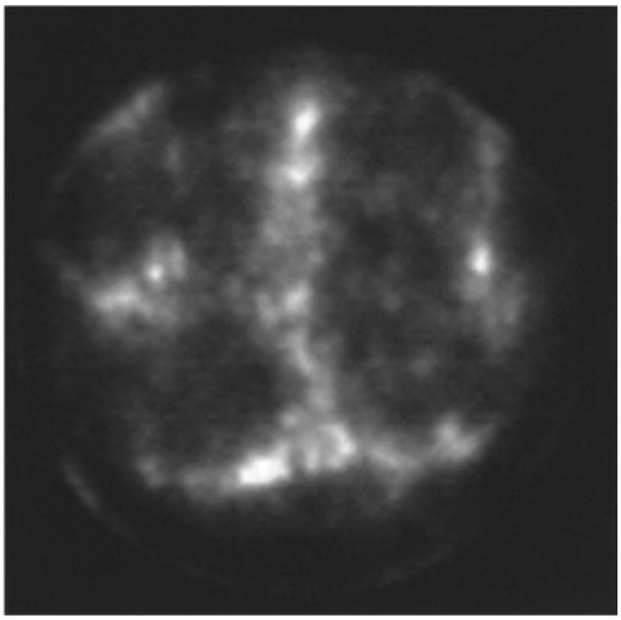

FIGURE 8. Typical pattern observed near onset ($R = 1.27$) in the random medium, cell D. Convection begins at $\Delta T = 7.91°$C.

3.2. *Results for cells B and C*

In order to better understand the origin of the roll orientation for cell A, we carried out experiments with cells B and C. Both of these cells have the same bar structure but have cylindrical horizontal planforms as shown in figure 1(*b*). Cell B is made from six bar layers, and cell C is made from seven bar layers. We show a typical result for cell B in figure 6. The roll orientation is 45° relative to the grid, as in cell A. In contrast to the pattern orientation of cell B, those of cell C are shown in figure 7. In the case of cell C, the rolls are always aligned perpendicular to the bars in the top and bottom layers. This result rules out the possibility that the orientation is due to forcing by the lateral boundaries. Indeed, the lateral boundaries appear to have a weaker influence than in moderate aspect ratio experiments for bulk-fluid Rayleigh–Bénard convection (Cross 1982). We might expect this difference because the bulk-fluid boundary condition is no slip while the porous-media boundary condition is best described as free slip (Joseph 1976).

We heuristically understand the difference between the patterns produced by the even and odd numbers of layers as follows. For an odd number of layers, the bars in the top and bottom layers are parallel. It is in these layers that the horizontal flow is strongest, so that the circulation should contain a vertical component and a component parallel to these bars. This causes the rolls to be oriented with their axes perpendicular to these bars. In the case of an even number of layers, the top and bottom sets of bars are perpendicular to each other. Were the pattern to align with either set of these bars, convection would be entirely suppressed in the other set. The roll orientation at 45° to either of these layers is the resulting compromise.

3.3. *Results for cell D*

The last of the three media types is the disordered medium which typically produces complicated cellular patterns such as that shown in figure 8. In this cell, convection

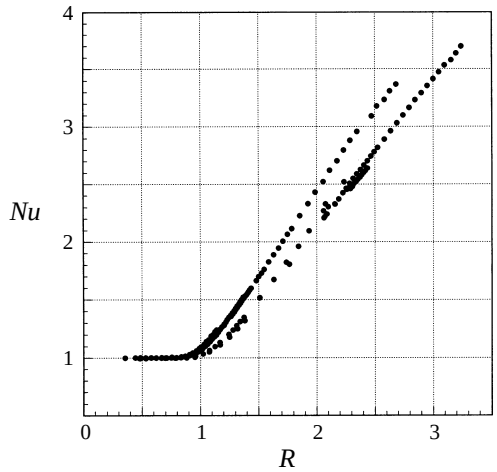

FIGURE 9. Nu versus R for five experimental runs in the disordered medium, cell D. The differences between the various curves are associated with different patterns produced by each run.

begins in small localized regions of the medium while flow in the rest of the medium remains quiescent. As the Rayleigh number increases, the pattern spreads outward from the seed areas, which remain as pinning sites for the pattern. That is, regions of initially strong flow remain so as the full pattern evolves. When the Rayleigh number is sufficiently high, convection occurs throughout the entire medium.

For cell D, we find that the measured value $Ra_c = 37 \pm 4$ is in good agreement with the expected critical Rayleigh number $Ra_c = 41.1$ (with corrections for anisotropy, see equation (1.1)). We use the point of intersection of the conductive and fully convective portions of the heat transfer curves (figure 9) to determine Ra_c. In the regime of R where convection fills the cell, the slope of $Nu(R)$ is 1.35 ± 0.15 (cell D) which is reasonably close to the prediction $S = 2$ (Joseph 1976). In the regime where only localized convection occurs, the Nusselt curve is rounded. The point where convection has spread throughout the medium is given approximately by the intersection of the constant-slope and rounded portions of the heat transfer curve. Since several different patterns occur, it is reasonable to expect that the Nusselt number will also differ from run to run. As shown in figure 9, each unique pattern produces a slightly different curve, $Nu(R)$, in the convective regime.

The critical wavenumber has a relatively large uncertainty because of the irregular nature of the pattern and the small aspect ratio. Its value, $q = 3.0 \pm 0.4$, is in agreement with theory within experimental error.

The cellular convection patterns strongly suggest that spatial variation in Ra plays a key role in the pattern selection, as proposed by Zimmermann *et al.* (1993). However, we cannot at this point exclude the possibility of some imperfection in the bifurcation associated with spatial variations in the thermal conductivity (Braester & Vadasz 1993). Since the regular media and the random media are equally Boussinesq and subject to identical boundary conditions at the top and bottom, it seems unlikely that the breaking of mid-plane symmetry from either of these two causes is responsible for the formation of the cellular patterns.

4. Conclusions

In this work, we describe in detail a modification of the shadowgraphic technique for studies of convection in porous media. This technique provides a simple method

for obtaining simultaneously the convective flow patterns and the heat transport for PMC. The present work and that of Shattuck *et al.* (1994, 1995, 1997) provide what are, to our knowledge, the first non-intrusive determinations of the horizontal flow patterns for PMC. These results provide new insights into PMC and raise a number of new issues which could not have been noted previously because of the lack of information concerning the flow pattern.

The key observation of these studies is that the structure of the medium plays a fundamentally important and previously unanticipated role in the determination of the flow pattern. In turn, this necessarily affects the heat transport, since this quantity is intrinsically dependent on the convective pattern. Thus, straight parallel rolls are not obtained in the disordered medium, even though that might most closely approximate an isotropic random porous medium. In addition, the structure of the regular media forces particular roll orientations.

The explanation for the effect of the solid matrix on the pattern selection lies in the fact that the pore scale cannot be chosen arbitrarily small compared to the other key length in the system, namely the height of the convection layer. Specifically, in designing an experiment, there must be a balance between the competing conditions that the pore scale be much smaller than the layer height, that the system be reasonably Boussinesq, and that the relaxation times be short enough to be tractable. For typical dense fluids such as water, and solid matrix constructions such as sphere packings, these conditions are mutually exclusive.

Since many past experiments have been constructed with nominally random pore structures, it is perhaps not surprising that cellular, i.e. localized, patterns have been typically observed. The measured rounding of the heat tranport seen in the disorderd media may also contain a contribution from horizontal spatial variations in the thermal conductivity of the media, leading to an imperfect bifurcation, as in Braester & Vadasz (1993). We emphasize that the present experiments are constructed so that there is effective mid-plane symmetry; hence there is no reason to believe that the cellular patterns are associated with breaking of this symmetry.

Since many (and possibly most) experimentally accessible PMC systems, including those studied here, fall into the regime for which the pore scale is smaller than the height, but not microscopically so, an important issue is the development of a modification of the existing theory which accounts for the inherent structure of the medium. One approach is to assume, as in recent studies (Gounot & Caltagirone 1989, Zimmermann *et al.* 1993, Braester & Vadasz 1993), that the medium properties, such as the permeability, the thermal conductivity or the Rayleigh number are functions of space. This is a convenient approach, which may shed some insight into the present observations. In particular, calculations of Zimmermann *et al.* with random spatial variations in *Ra* are in good qualitative agreement *vis-à-vis* the localization of the patterns, and in reasonable quantitative agreement *vis-à-vis* the heat transport with the present experiments. However, variability in the primary parameters such as κ_m or γ may be qualitatively different from variability in *Ra*. This difference occurs for two reasons. The first is that in the equations of motion κ_m and γ are subject to spatial gradients, directly or as part of the reduction of the equations of motion, whereas *Ra* in the analysis of Zimmermann *et al.* is not. The second is that spatial variations in the effective conductivity can (but do not necessarily) lead to an imperfect bifurction, as shown by Braester & Vadasz. We will present elsewhere theoretical studies which focus directly on the variability of k_m or γ at the pore scale.

A particularly interesting feature of these experiments and those of Shattuck *et al.* (1994, 1995, 1997) is that well-defined roll-like patterns occur typically for media

with an ordered spatial structure. At this time, we do not know of a theory which takes into account such periodic structure. Nevertheless, the roll states which evolve for the regular media are, in many regards, in agreement with standard theoretical models which assume a homogeneous system. Specifically, for the MST experiments, the wavenumber, critical Rayleigh number, and stability properties are consistent with theory, particularly given that the experiments pertain to relatively small aspect ratios. Clearly, studies with larger aspect ratios would be useful in this regard. The heat transport slope for the regular media is smaller by about a factor of 4 than predictions, but again the effects of aspect ratio may be important. It is interesting that the corresponding slope for the random media is much closer to the predictions for homogeneous media.

Regarding porous media which vary periodically in space, it is possible to provide a direction for theory and for future experiment. Specifically, if the pore structure is periodic with wavevector k, then, at onset, the linearized solutions will have a Floquet form for the velocity and temperature: $\exp(\mathrm{i}qx)U(x)$, where U is periodic in space with period determined by k. The effect of the lattice may be particularly important for PMC with a binary mixture. In that case, both oscillatory modes and stationary modes can occur. The nature of these modes may be strongly affected by the periodicity of the matrix in the parameter regime in which the critical Rayleigh numbers for the two kinds of modes are comparable.

We would like to gratefully acknowledge the support of the National Science Foundation under grant numbers CTS-90-06189, CTS-91-57910, and CTS-93-07197 and the North Carolina Supercomputing Center.

REFERENCES

Amiri, A. & Vafai, K. 1994 Analysis of dispersion effects and non-thermal equilibrium, non-Darcian, variable porosity incompressible flow through porous media. *Intl J. Heat Mass Transfer* **37**, 939–954.

Beck, J. L. 1972 Convection in a box of porous material saturated with fluid. *Phys. Fluids* **15**, 1377–1383.

Braester, C. & Vadasz, P. 1993 The effect of a weak heterogeneity of a porous medium on natural convection. *J. Fluid Mech.* **254**, 345–362.

Castinel, G. & Combarnous, M. 1975 Natural convection in an anisotropic porous layer. *Rev. Gén. Therm.* **168**, 937–947.

Close, D. J., Symons, J. G. & White, R. F. 1985 Convective heat transfer in shallow gas-filled porous media: experimental investigation. *Intl J. Heat Mass Transfer* **28**, 2371–2378.

Cross, M. C. 1982 Ingredients of a theory of convective textures close to onset. *Phys. Rev.* A **25**, 1065–1076.

Elder, J. W. 1967 Steady free convection in a porous medium heated from below. *J. Fluid Mech.* **27**, 29–48.

Epherre, J. F. 1975 Criterion for the appearance of natural convection in an anisotropic porous layer. *Rev. Gén. Therm.* **168**, 949–950.

Gounot, J. & Caltagirone, J. P. 1989 Stabilité et convection naturelle au sein d'une couche poreuse non homogène. *Intl J. Heat Mass Transfer* **32**, 1131–1140.

Howle L. E. 1993 Pattern formation at the onset of convection in porous media. PhD thesis, Duke University, Durham.

Howle, L. E., Behringer, R. P. & Georgiadis, J. G. 1993*a* Shadowgraphic visualization of natural convection in rectangular-grid porous layers. In *Topics in Heat Transfer I* (ed. M. Keyhani *et al.*). HTD, vol. 206, pp. 17–23.

Howle, L. E., Behringer, R. P. & Georgiadis, J. G. 1993*b* Visualization of convective fluid flow in a porous medium. *Nature* **362**, 230–232.

Howle, L. E. & Georgiadis, J. G. 1994 Natural convection in porous media with anisotropic dispersive thermal conductivity. *Intl J. Heas Mass Transfer* **37**, 1081–1094.

Joseph, D. D. 1976 *Stability of Fluid Motions II*. Springer.

Kvernvold, O. & Tyvand, P.A. 1979 Nonlinear thermal convection in anisotropic porous media. *J. Fluid Mech.* **90**, 609–624.

Lide, D. R. & Frederikse, H. P. R. (eds.) 1994 *CRC Handbook of Chemistry and Physics* 75*th* Edn. CRC Press, Boca Ratan.

Lister, C. R. B. 1990 An explanation for the multivalued heat transport found experimentally for convection in a porous medium. *J. Fluid Mech.* **214**, 287–320.

Metcalfe, G. P. & Behringer, R. P. 1991 Rayleigh numbers for cryogenic experiments. *J. Low Temp. Phys.* **78**, 231–246.

Néel, M. C. 1990 Convection in a horizontal porous layer of infinite extent. *Eur. J. Mech.* B *Fluids* **9**, 155–176.

Shattuck, M., Behringer, R. P., Johnson G. A. & Georgiadis, J. G. 1994 Magnetic resonance imaging of convection in porous media In *Twelfth Symp. on Energy Engineering Sciences,* pp. 64–74.

Shattuck, M., Behringer, R. P., Johnson G. A. & Georgiadis, J. G. 1995 Onset and stability of convection in porous media: Visualization by magnetic resonance imaging. *Phys. Rev. Lett.* **75**, 1934–1937.

Shattuck, M., Behringer, R. P., Johnson G. A. & Georgiadis, J. G. 1997 Convection and flow in porous media. Part 1. Visualization by magnetic resonance imaging. *J. Fluid Mech.* **332**, 215–245.

Straus, J. M. 1974 Large amplitude convection in porous media. *J. Fluid Mech.* **64**, 51–63.

Swift, J. & Hohenberg, P.C. 1974 Hydrodynamic fluctuations at the convective instability. *Phys. Rev.* A **15**, 319–328.

Vafai, K. 1984 Convective flow and heat transfer in variable-porosity media. *J. Fluid Mech.* **147**, 233–259.

Vincourt, M. C. 1989 Influence of a heterogeneity on the selection of convective patterns in a porous layer. *Intl J. Engng Sci.* **27**, 377–392.

Zimmermann, W., Seeβelberg, M. & Petruccione, F. 1993 Effects of disorder in pattern formation. *Phys. Rev.* E **48**, 2699–2703.